ELSEVIER

Materials Science and Engineering A359 (2003) 158–167

MATERIALS SCIENCE & ENGINEERING A

www.elsevier.com/locate/msea

Effect of deposition conditions on mechanical stresses and microstructure of sputter-deposited molybdenum and reactively sputter-deposited molybdenum nitride films

Y.G. Shen *

Department of Manufacturing Engineering and Engineering Management (MEEM), City University of Hong Kong, Tat Chee Avenue, Kowloon, Hong Kong

Received 25 April 2002; received in revised form 14 April 2003

Abstract

A combined investigation of mechanical stress generation by in situ substrate curvature measurements during the growth of MoN_x thin films, with $0 \leq x \leq 0.35$, and of structural properties by ex situ X-ray diffraction (XRD), transmission electron microscopy (TEM), transmission electron diffraction (TED), X-ray photoelectron spectroscopy (XPS), and electron energy-loss spectroscopy (EELS) is reported. It was found that the Mo film stresses strongly depended on the Ar sputtering pressure and changed from highly compressive to highly tensile in a relatively narrow pressure range of 6–12 mTorr. For pressures exceeding ~40 mTorr, the stress in the film was nearly zero. Cross-sectional TEM measurements indicated that the compressively stressed films contained a dense microstructure without any columns, while the films having tensile stress had a very columnar microstructure. High sputtering-gas pressure conditions yielded dendritic-like film growth, resulting in complete relaxation of the mechanical tensile stresses. It was also found that the properties of the deposited MoN_x films depended not only on the nitrogen partial pressure in Ar–N_2 gas mixtures but also on the total sputtering-gas pressure. Cross-sectional TEM studies showed that an average column width for 160 nm-thick films near stoichiometry of Mo_2N was about ~15–20 nm. Using the electron scattering data collected from a range of crystalline samples for calculating the pair distribution function (PDF) by Fourier transformation in real space, Mo–N and Mo–Mo bonding in the films was also identified. Once the Mo_2N phase was formed, the density, microstructure and bonding feature were similar and insensitive to the total sputtering pressure used in this study.

Keywords: Microstructure; Molybdenum; Molybdenum nitride; Reactive magnetron sputtering; Stress

1. Introduction

Thin films of molybdenum (Mo) and molybdenum nitride (MoN_x) have been extensively used in various technological areas, especially as diffusion barriers in microelectronics, hard wear-resistant materials in engineering, and interconnections in semiconductor devices. All these applications are due to their remarkable properties such as high hardness, high melting point, good chemical stability and high conductivity [1]. Accordingly, a considerable number of detailed investigations has been carried out on the deposition and characterization of molybdenum [2–5] and molybdenum nitride [6–12] films by employing a variety of techniques, such as dc/rf magnetron sputtering, chemical vapor deposition, laser-promoted nitridation, ion-beam assisted deposition, and reactive magnetron sputtering. Characterization was based primarily upon electrical resistivity, chemical-state configuration of elements, phase identification, and surface morphology as a function of processing conditions. Currently, physical vapor deposition of thin films onto various substrates is the most popular technique for synthesizing Mo and MoN_x because these films are easily and reproducibly formed by magnetron sputtering or reactive magnetron sputtering from a pure Mo target in an Ar or an Ar–N_2 gas mixture. However, very little is known today about

* Tel.: +852-2-784-4658; fax: +852-2-788-8423.
E-mail address: mcshen@cityu.edu.hk (Y.G. Shen).

0921-5093/03/$ - see front matter
doi:10.1016/S0921-5093(03)00336-8

the effect of deposition conditions on mechanical stress and microstructure of Mo and MoN_x films.

In the present study, the effect of deposition conditions on mechanical stress and microstructure of thin Mo and MoN_x films is presented, in which some new features not reported in previous studies of these systems have been revealed. Direct measurements of the stress evolution in real time during magnetron sputtering of Mo and reactive magnetron sputtering of MoN_x were carried out using a wafer curvature-based technique. Extensive spectroscopic measurements were also performed using X-ray diffraction (XRD), transmission electron microscopy (TEM), transmission electron diffraction (TED), X-ray photoelectron spectroscopy (XPS), and electron energy-loss spectroscopy (EELS).

2. Experimental details

MoN_x films, with $0 \leq x \leq 0.35$, were deposited on unheated Si(100) substrates by reactive dc magnetron sputtering of a 99.99% pure tungsten disk (50 mm in diameter). The system has been described previously [13,14]. Briefly, depositions were made with a constant magnetron current of 0.28 A, which required a discharge voltage of $\sim$300 V, independent on the gas mixture. Prior to deposition, the system was evacuated to a pressure of 3×10^{-6} Torr and then an Ar/N_2 gas flow controlled using two independent mass flow controllers was admitted into the chamber. The ratio of N_2 to $Ar+N_2$ could be changed, so as to vary nitrogen concentration x. The substrates were 330 μm-thick silicon with dimensions 10×10 mm^2, cleaved from 76 mm wafers of p-type (100) silicon ($\rho \sim 1$–10 Ω cm). The target was sputter cleaned for 5 min with a shutter covering the substrate, prior to initiating deposition. The target-to-substrate spacing was 70 mm.

Unless otherwise illustrated, all films were deposited to a nominal thickness of 160 nm. The thickness of the films was determined using stylus profilometry (Tencor P-10) and confirmed by cross-sectional TEM measurements. Substrate temperature during film growth was estimated to be 150 °C including plasma heating. These samples will be denoted as as-deposited samples. Post-deposition annealing of the samples was carried out in a vacuum of better than 5×10^{-7} Torr in the temperature range of 100–750 °C. Annealing time was 30 min.

The crystallographic structure of the films was determined by XRD using a Siemens D5000 diffractometer with a Cu tube operated at 40 kV and 30 mA. The measurements were carried out using Cu Kα radiation with a Ni filter to remove Cu Kβ reflections. The cross-sectional TEM images were obtained in a Phillips EM430 microscope operated at 300 kV. The atomic concentrations of elements as well as their chemical bonding were investigated by XPS using a Kratos Axis/800 hemispherical energy analyzer equipped with an unmonochromatized Mg Kα X-ray source ($h\nu = 1253.6$ eV). The binding energy scale was calibrated against Ag $3d_{5/2}$ at 368.25 eV and the instrumental energy resolution, measured using the same peak, was 0.9 eV (pass energy set at 20 eV). Charging corrections were made using the as-measured Fermi level of Ag and Au pieces on the metallic substrate holder using the Mg Kα radiation as a reference. The density of the films was analyzed by EELS in a Phillips EM430 TEM equipped with a GATAN 666 parallel electron energy-loss spectrometer operated at 300 keV. All electron energy-loss measurements were carried out in diffraction mode (image coupling to the spectrometer) with a collection angle of $\sim$8 mrad. Contamination of the beams under the electron beam was found not to be a problem when using a defocused probe and an area-selecting aperture.

Cross-sectional specimens were prepared by gluing two samples face-to-face with epoxy resin and then mechanically thinning from both sides to 30 μm followed by 3 keV Ar^+-ion milling at 8° with respect to the specimen surface to obtain electron transparency. A range of samples was also deposited onto the NaCl substrates and then floated off for TED and EELS measurements.

3. Results

3.1. In situ mechanical stress measurements, cross-sectional TEM and TED

The development of film stress during deposition was determined with a vacuum cantilever beam apparatus using an optical two-beam deflection method to detect changes in the substrate curvature. The film stress σ is obtained by the well-known Stoney's equation revised for biaxial stress,

$$\sigma = \frac{1}{6} \frac{E_s h_s^2}{(1-\nu_s) h_f} \left[\frac{1}{r} - \frac{1}{r_0} \right] \quad (1)$$

where $E_s/(1-\nu_s)$ is the biaxial modulus of the substrate, h_s and h_f are the thickness of the substrate and film, and r_0 and r denote the curvature radii before and after film deposition, respectively. The substrate curvature was measured on a beam-shaped sample by deflection of a splitted laser beam from both ends. The sample stripes were 2 mm wide and 18 mm long. They were cut from the Si(100) wafers [$h_s = 85$ μm, $E_s/(1-\nu_s) = 180.5$ GPa]. It has been verified that the original curvature of a bare silicon wafer is negligible compared with the measured curvatures after deposition.

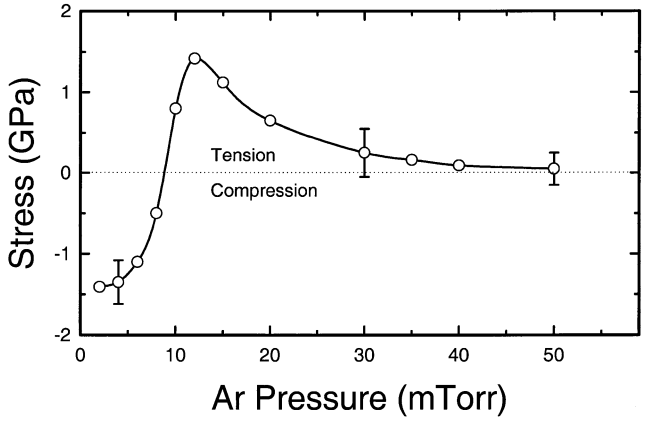

Fig. 1. Mechanical stress in 160 nm-thick Mo films as a function of Ar sputtering-gas pressure.

The measurement reveals how the Ar sputtering-gas pressure influences the formation of mechanical stresses in the Mo films. Fig. 1 shows the evolution of the mechanical stress for a series of Mo films as a function of sputtering-gas pressure. In our study, the power density was fixed, and the only variable was the Ar pressure. No delamination of the films was observed in all cases. In the low-pressure range of 2–6 mTorr, the Mo films are subjected to high compressive stresses. As the sputtering-gas pressure is increased, the stress changes from compression to tension, reaching a maximum (1.42 GPa) at 12 mTorr, and with further increase the stress is gradually decreased. For pressures exceeding about 40 mTorr the stress in the film is nearly zero. This dependence of mechanical stress on sputtering-gas pressure shown in Fig. 1 has already been reported in many other refractory-metal films, such as Cr and W [15–17], deposited by dc and rf magnetron sputtering using ex situ XRD $\sin^2\psi$ method and curvature-based techniques.

The evolution of the microstructure of the Mo films with sputtering-gas pressure has been investigated by examining the cross sections in comparable thickness films by means of cross-sectional TEM. Fig. 2 shows bright-field cross-sectional TEM micrographs from three different Mo films. It was found that the films deposited at a low pressure of 2 mTorr (compressive stress, Fig. 1) contains a dense microstructure without any columns shown in Fig. 2a. No evidence of the presence of voids in compressive stress films was observed. Most of the microstructure is composed of large bcc Mo grains. The coarse bcc grains are also evident from the spotty rings obtained from TED (not shown). For a film deposited at 12 mTorr (maximum tensile stress, Fig. 1), a very columnar microstructure is observed (Fig. 2b). It is interesting to note that the surface structure in Fig. 2b has changed compared with that in Fig. 2a, each column having a domed top. At a high pressure of $\sim$40 mTorr, where the stress is nearly

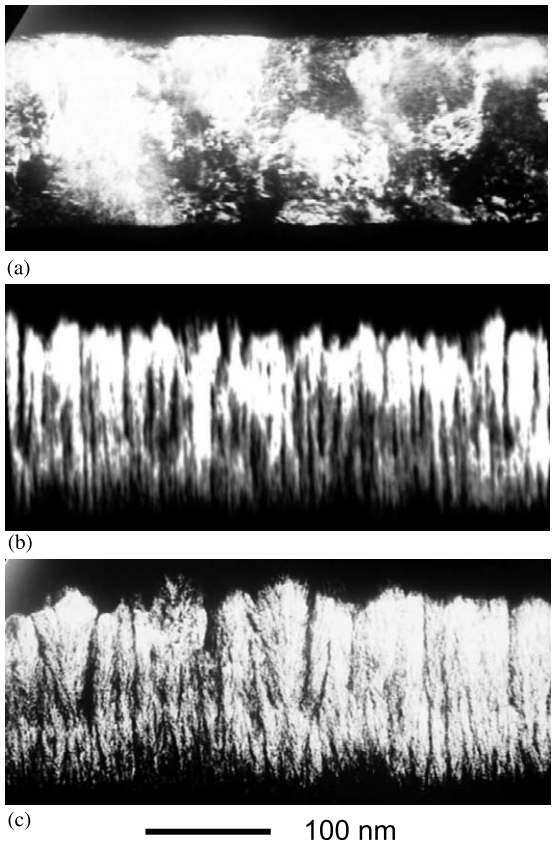

Fig. 2. Cross-sectional TEM images showing the microstructure evolution of three Mo thin films deposited under different Ar sputtering-gas pressures (the corresponding stress values are given in Fig. 1); (a) at 2 mTorr, (b) at 12 mTorr, and (c) at 40 mTorr.

zero, the columnar microstructure has disappeared and a dendritic-like structure is observed (Fig. 2c). Compared with the tensile stress film in Fig. 2b, the amount of column boundary voids and the extent of surface roughness are more dramatic. The electron diffraction pattern obtained from the zero stress film shows an amorphous feature. This is in good agreement with the XRD measurements (not shown). These results clearly show that the mechanical stress level in the Mo films deposited under different Ar sputtering pressures is strongly correlated to their microstructure.

Fig. 3 shows the evolution of mechanical stresses in a series of MoN_x films deposited under three different total pressures ($Ar+N_2$) as a function of x. In a low pressure of 4 mTorr (Fig. 3a), the films without nitrogen addition are under high compressive stresses (1.38 GPa). As the nitrogen content increases, a decrease in film compressive stress is observed. This stress change is due to variations in both the average impact energy of sputtered Mo atoms and accelerated ions incident at the growing film. The compressive stress has a value of $\sim$ 0.85 GPa for films near stoichiometry of Mo_2N. In a higher pressure of 12 mTorr (Fig. 3b), the tensile stress (1.42 GPa) was observed in a pure Mo film. The stress

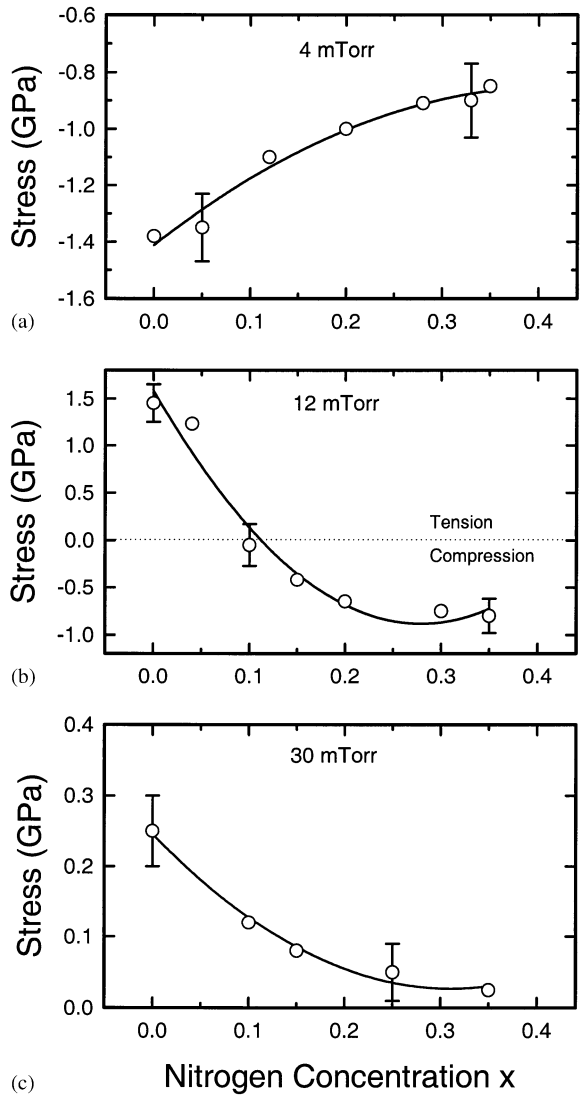

Fig. 3. Mechanical stresses of as-deposited MoN_x films prepared under three different Ar sputtering-gas pressures as a function of x; (a) at 4 mTorr, (b) at 12 mTorr, and (c) at 30 mTorr.

becomes smaller by introducing a small amount of N_2 in the sputtering chamber and reaches nearly zero at x = 0.1. Beyond this point, the stress turns to be compressive. The compressive stress has a value of 0.8 GPa for a film with x = 0.35. At a high pressure, ~30 mTorr, the Mo film has a lower tensile stress of 0.25 GPa. As x increases, the structure collapses into a disordered amorphous network with a decrease in film stress as observed (Fig. 3c). At x = 0.35, the film is almost free of mechanical stress.

Typical cross-sectional TEM image obtained from a Mo_2N film deposited at a total pressure of 4 mTorr after annealing to 500 °C is shown in Fig. 4a. It can be seen that the film contains a well-defined columnar microstructure with uniform columns from substrate to top of the films. The column boundaries appear to be decorated by a relatively low density of voids. The average

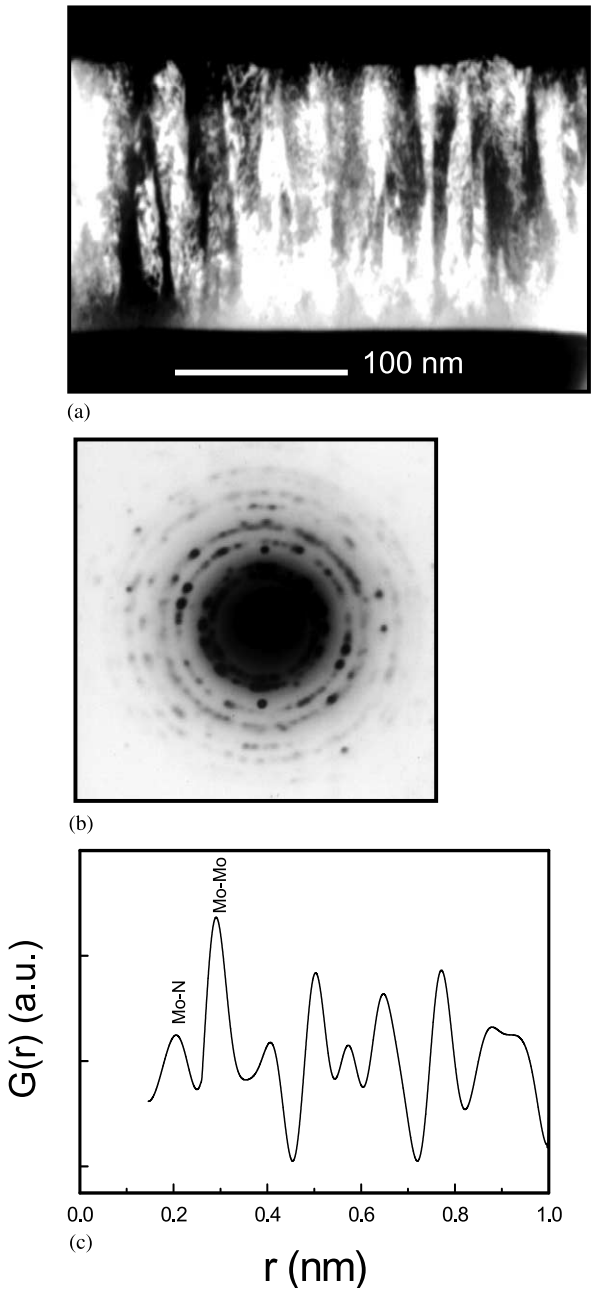

Fig. 4. (a) Cross-sectional TEM image of a MoN_x film with x = 0.35 and (b) the TED pattern from the same film. (c) The experimental G(r) obtained by Fourier transformation of the reduced TED intensity S(q) from the MoN_x film at x = 0.35 after annealing to 500 °C. The film thickness was 50 nm.

column diameter is about 15–20 nm. The electron diffraction pattern of the film (see Fig. 4b) clearly shows the (111), (200), (220), (311), (222), (331) and (420) diffraction rings for fcc Mo_2N.

Structure in a crystalline Mo_2N is essentially of a long-range nature and is best described by the pair distribution function (PDF), which gives a measure of nearest neighbor distances between atoms. It is well known that electrons are scattered more strongly by matter than by X-rays or neutrons. This property allows

diffraction analysis of micro-volumes of solids with good statistics and renders electrons a unique technique in the study of thin films. In this study, TED intensities I(q) were collected using a Phillips EM430 TEM fitted with a GATAN 666 parallel EELS operating at 300 kV. The PDF, denoted G(r), is calculated as Fourier transformation of the reduced TED intensities $S(q) = q[I(q)/Nf^2 - 1]$ in real space [see our recent publications in [13,14] for details of the method]:

$$G(r) = 8\pi \int_0^{q_{max}} \frac{q[I(q) - Nf^2]}{Nf^2} W(q)\sin 2\pi rqdq \quad (2)$$

where N is the number of atoms in the compound, f is the atomic scattering factor, and $W(q) = \sin(\pi q/q_{max})/(\pi q/q_{max})$ is the Lorch damping function. The scattering factor $q = 2 \sin \theta/\lambda$ was collected to a maximum value of q, q_{max}, of 3.5 $Å^{-1}$.

For a binary system, the G(r) function is a sum of all the partial PDFs, $g_{m,n}(r)$, between two types of atom, m and n:

$$G(r) = 4\pi r\rho_0 \sum_{m,n} W_{m,n}[g_{m,n}(r) - 1] \quad (3)$$

where ρ_0 is the average atomic density, and the weighting factors, $W_{m,n} = c_m c_n f_m f_n$, depend on both the atomic fraction, c, and the effective atomic scattering factor, f, of the binary system. For a MoN_x film, the average atomic scattering factor f is defined to be $(1-c)f_N + cf_{Mo}$ where c is the Mo content, and f_{Mo} and f_N are the kinematic electron scattering factors of Mo and N as given in the literature [19]. The G(r) of the film obtained by Fourier sine transformation of the reduced TED intensity S(q) gives accurate atomic distances up to the first seven nearest neighbours within 0.02 Å. Our measurements provide unambiguous identification of Mo–N and Mo–Mo bonding in the films.

3.2. XRD

Our XRD $\theta-2\theta$ measurements indicate that the crystallographic structure of reactively sputter-deposited MoN_x depends on the concentration of nitrogen, x, in the films. At low values of x (< 0.08), the films contain mainly bcc Mo. A two-phase structure consisting of bcc Mo and fcc Mo_2N is observed in the range of $x = 0.10$–0.26. When x reaches 0.28 or up to 0.35, a single fcc Mo_2N phase is observed. In Fig. 5, the XRD $\theta-2\theta$ scans show that the lattice parameter of the films increases from 0.3147 to 0.4195 nm while nitrogen concentration x increases from 0 to 0.35. The points labeled A, B, and C gave the XRD patterns collected from as-deposited films shown. For a film without containing N, a bcc Mo structure is observed with a (110) preferred orientation because the (110) planes are closest-packed in bcc Mo with the lowest surface energy. At higher values of x, the lattice constants [calculated from the (111) peak positions] are higher than the bulk value of Mo_2N, 0.4163 nm [18]. This is attributed to the expansion of lattice constant by the incorporation of nitrogen atoms. It is also noted that at higher nitrogen concentrations, the diffraction peaks are broad and their intensities are weak. These results indicate that the crystalline Mo_2N structure of the films formed at low temperatures is less ordered, probably due to small crystal sizes and distortion of the cubic lattice structure. Annealing of the as-deposited films resulted in an improved crystallinity of the Mo_2N structure, which is related to the N concentration. After annealing to 500 °C, the lattice parameters approach to reported bulk value of 0.4163 nm, indicating that the layers are nearly fully relaxed.

Our XRD measurements also reveal that the fcc Mo_2N structure is stable up to 750 °C. Fig. 6 shows a detailed XRD $\theta-2\theta$ scan for 2θ angles up to 150° obtained from a MoN_x film after annealing to 750 °C. For the film at $x = 0.35$ (close to stoichiometry of Mo_2N), the diffraction lines showing a single-phase structure of Mo_2N are observed. The major trend is growth with a (111) preferred orientation. The (111) orientation is favored most likely because the (111) planes are closest-packed in the fcc Mo_2N structure with the lowest surface energy. After higher temperature annealing adatom mobilities in the film are sufficiently high to favor crystallites bounded by low energy planes. The major peaks observed at angles 2θ equal to 37.56, 43.66, 63.64, 75.8, 79.96, 95.41, 108.04, 111.72 and 130.55°. These peaks are assignable to (111), (200), (220), (311), (222), (400), (331), (420) and (422) reflections of fcc Mo_2N structures.

3.3. XPS and EELS

XPS techniques permits to identify elements and their chemical states present in the outermost ~ 5 nm of the surface of the samples. During the operation and transfer into the spectrometer preparation chamber, the surface of the film samples was exposed to air prior to the XPS measurement (as were all of the samples) and, therefore, contained surface oxide. Survey spectra from these films revealed, in addition to the dominant Mo, N, and O related peaks, a very small C 1s peak was also present and disappeared after the sample was irradiated with a small Ar ion dose. Fig. 7a and b show typical XPS spectra of the films in the Mo 3d and N 1s energy regions, respectively. These spectra were obtained from two fcc Mo_2N films prepared under different total pressures after annealing to 500 °C. For comparison, the spectrum of a bcc Mo film in the Mo 3d energy region is also shown in Fig. 7a. For the as-deposited Mo_2N film prepared at 4 mTorr (Fig. 7a), Mo $3d_{5/2}$ and Mo $3d_{3/2}$ peaks are situated at higher positions

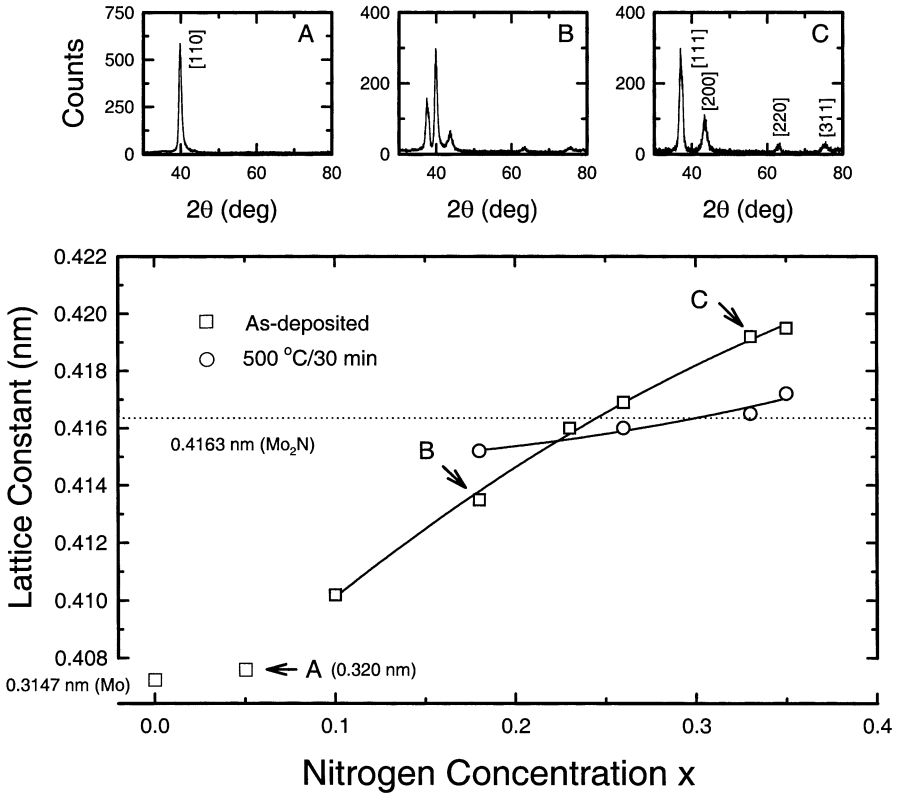

Fig. 5. Variation of lattice parameters in MoN_x films as a function of x before and after annealing to 500 °C. The XRD θ−2θ patterns labeled A, B, and C obtained from as-deposited films at x = 0.05, 0.18, and 0.33, respectively, are also shown.

at 228.5 and 232.2 eV, respectively. The peak at 235.5 eV overlaps with that of the oxide. After sputter etching, the binding energies of the film (at a depth of approximately 8 nm, curve A) are shifted to energies at 228.1 and 231.4 eV. The chemical shifts in the core levels of the Mo_2N film relative to elemental Mo (centered at 227.8 and 231.0 eV) reflect a charge transfer from molybdenum to nitrogen during the nitridation process. Similar chemical shifts were also observed for the film prepared at 12 mTorr (curve B). In addition, the

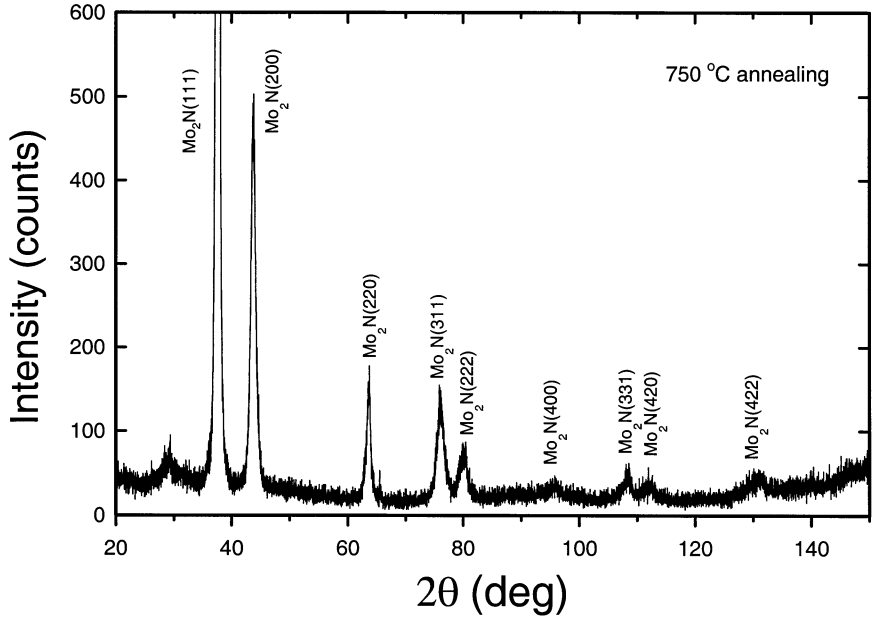

Fig. 6. XRD θ−2θ scan from a MoN_x film with x = 0.35 after annealing to 750 °C.

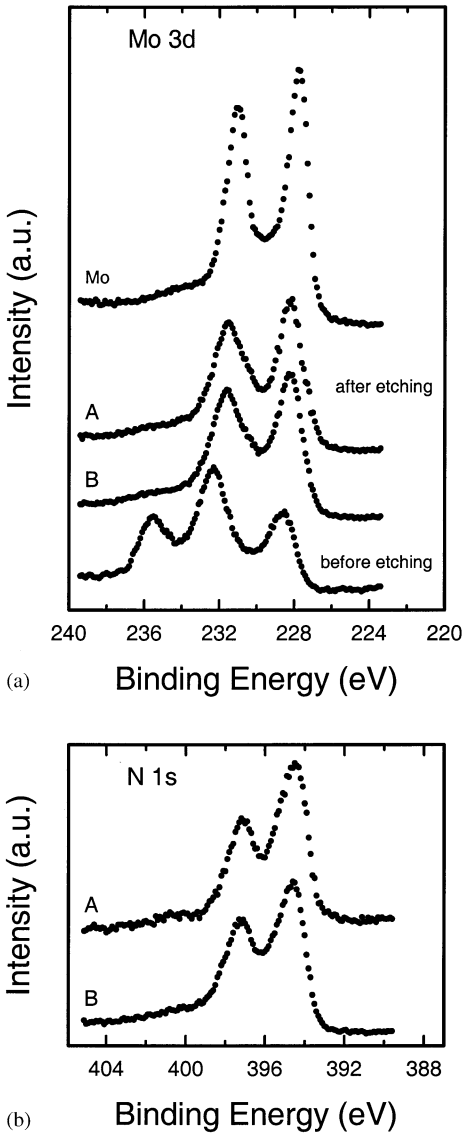

Fig. 7. Typical XPS (a) Mo 3d and (b) N 1s spectra in Mo_2N films. The films were deposited at total sputtering-gas pressures of 4 (curve A) and 12 mTorr (curve B), respectively. For comparison, Mo 3d spectrum from a bcc Mo film after sputtering etching is also shown in (a). Etching time was 3 min. The Mo and Mo_2N films were annealed to 500 °C. Curves have been offset vertically for clarity.

fact that the N 1s spectra showed two peaks centered at 394.5 and 397.2 eV for 4 mTorr case and 394.6 and 397.5 eV for 12 mTorr case (Fig. 7b), is assigned to Mo 3p–N 1s [20].

EELS have been shown to be a useful tool in the determination of film density and the quantitative analysis of chemical impurities. Typical EELS low-loss spectra obtained from a Mo_2N film prepared at 4 mTorr before and after annealing to 600 °C are shown in Fig. 8a. The low-loss spectra have been deconvoluted with the zero-loss peak. For the as-deposited film (curve A), the spectrum shows the surface and bulk plasmon loss peaks centered at ~10.3 and 21.0 eV, respectively. The

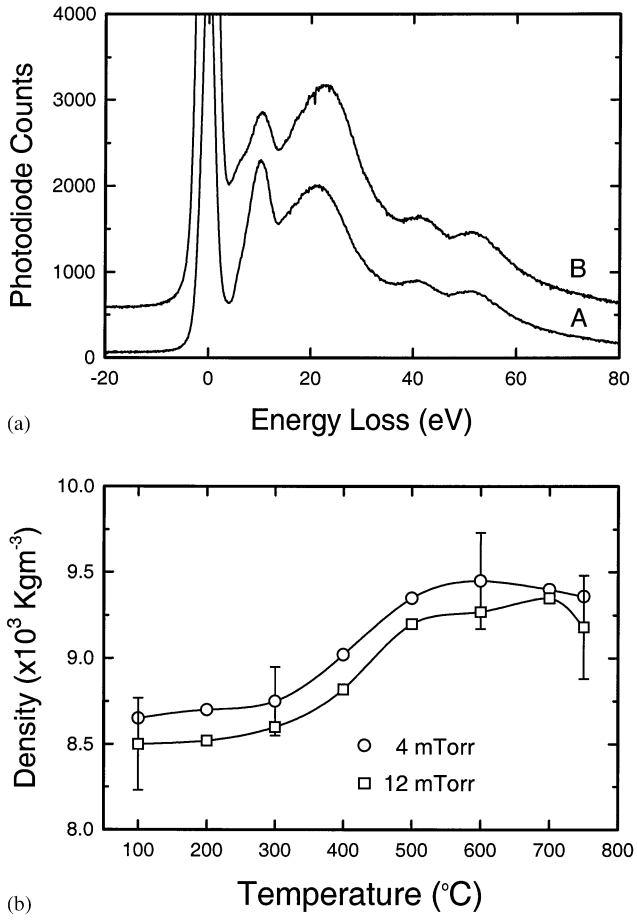

Fig. 8. Typical electron energy zero-loss spectra obtained from a film prepared at 4 mTorr before (curve A) and after (curve B) in situ annealing to 600 °C for 20 min. (b) Mass density of the two Mo_2N films prepared under two different pressures as a function of annealing temperature.

high-energy loss features at 40.7 and 52.8 eV are attributed to interband transition from the Mo 4s and Mo 4p orbitals, respectively, to unoccupied states near the Fermi level E_F [21]. The zero-loss spectrum for the annealed film (curve B) is similar to that of the as-deposited film. It is noted that the bulk plasmon loss peak after annealing is shifted to a higher position centered at 22.3 eV (curve B), while no loss of the N content in the film was evidenced. This is due to the fact that annealing the film to a higher temperature provides sufficient atomic mobility for both Mo and N atoms to reach sides, which are conducive to a densely packed crystalline structure.

The energy E_p of the bulk plasmon loss peak is related to the valence electron density n_e using the free-electron formula [21]:

$$E_p = \hbar\left[n_e \frac{e^2}{m^*\varepsilon_0}\right]^{\frac{1}{2}} \quad (4)$$

where m* is the effective electron mass and $\hbar$, e, ε_0 have

their usual meanings. Considering the molybdenum 4d and 5s orbitals and nitrogen 2s and 2p orbitals, we assume that molybdenum and nitrogen contribute six and five valence electrons per atom, respectively, to the valence electron plasmon. Therefore, the electron density is given by:

$$n_e = 6n_{Mo} + 5n_N \quad (5)$$

where n_{Mo} and n_N are the concentrations of molybdenum and nitrogen atoms, respectively. Using Eqs. (4) and (5) the density of Mo_2N films can be measured using the value of the bulk plasmon energies determined from EELS low-loss spectra. Fig. 8b shows the mass densities of the two films obtained under different sputtering pressures as a function of annealing temperature.

4. Discussion

4.1. Mechanical stress and microstructure

The mechanical stress and microstructure of the films are influenced by changing sputtering pressure through ion bombardment. We have shown that the mechanical stress is an important parameter, which either correlates with, or directly influences, most of the structural properties of sputter-deposited Mo films. The features observed in the plots of Figs. 1 and 2 are a manifestation of the correlation of the stress and microstructure. At low sputtering pressures, the films contain a dense microstructure without any columns which is responsible for the observed compressive stress (Fig. 1 and Fig. 2a). Usually, the occurrence of mechanical stress is due to the atomic peening effect [22] caused by energetic particles such as sputtered atoms and sputtering-gas atoms or ions, leading to densification of the microstructure. The sputtered atoms normally arrive at the surface of the growing film with enhanced energy. These energetic particles strike the surface, limiting the development of a columnar growth morphology. With increasing Ar pressures, the films obtained show a columnar microstructure and developed a tensile stress (Fig. 1 and Fig. 2b). The columnar structure observed for the tensile stress films indicates the presence of voids in the material. This type of defect tends to shrink the films due to the high surface tension of the inner surface of the voids. As a result, the film volume decreases and tensile stress is generated. The films deposited at high sputtering pressures show a dendritic-like microstructure (Fig. 2c). It is evident that open columnar structures are unable to support large mechanical stress in the film.

For reactively sputter-deposited MoN_x films, it is found that their properties depend not only on the nitrogen partial pressure in $Ar–N_2$ gas mixtures but also on the total sputtering-gas pressures (Fig. 3). The initial compressive stress observed in a low sputtering-gas pressure of 4 mTorr becomes smaller by introducing a small amount of N_2 in the sputtering chamber (Fig. 3a). It suggests that the stress depends mainly on the N content in the MoN_x films. This relaxation of compressive stresses may, therefore, be understood in terms of a loss in inter-grain coupling as a result of increased porosity in the grain boundaries followed by development of a two-phase network and then one-phase structure as the nitrogen increases. In a higher sputtering-gas pressure of 12 mTorr, the film initially showed a tensile stress corresponding to a columnar microstructure (Fig. 3b). The stress moves toward compressive by increasing the nitrogen content. It seems reasonable to assume that the interstitial N atoms incorporated causes the lattice expanded, resulting in compressive stress in the films. The films deposited at 30 mTorr without nitrogen addition show a low tensile stress (Fig. 3c). The growth of amorphous films in the absence of substantial energetic particle bombardment is known to result in underdense films, which are unable to support large mechanical stress. As the nitrogen content increases, a completely disordered amorphous MoN_x network develops, leading to nearly zero value of tensile stresses.

The columnar nature of the microstructure in the Mo_2N films has been demonstrated using cross-sectional TEM (Fig. 4a). The columnar microstructure may develop by surface diffusion process influenced by both geometrical shadowing effects and limited atomic mobility. The 160 nm-thick films have a columnar microstructure with an average column width near the surface of 15–20 nm. From the image, we see that the column boundaries appear to be decorated by a relatively low density of voids. The absence of doming at the top side of the film is indicative of a less well-defined columnar morphology. We have also shown that TED with a PDF analysis is a powerful technique, which is capable of detecting the structure of cubic Mo_2N compound, and producing quantitative data of the Mo–N and Mo–Mo atomic distance parameters (Fig. 4c).

4.2. Film structure and thermal stability

At a lower growth temperature, atomic displacement, local atomic arrangements, and enhancement of adatom mobilities are limited. Our XRD $\theta-2\theta$ measurements indicate that in N_2 deficient ambient or at lower values of x, the 160 nm films contained mainly bcc Mo, while in the $0.10 \leq x \leq 0.26$ range, the films had a two-phase structure consisting of bcc Mo and fcc Mo_2N. When the x value reached 0.28 or above, the films had an ordered crystalline Mo_2N structure. It is apparent from these results that the dominant processes in sputter deposition which control the kinetics and mechanisms during film growth are changing at different Ar to N_2 partial pressures. For deposition at a low pressure of 4 mTorr,

penetration, local atomic rearrangements, and atomic displacements increase and the original Mo particles as well as Mo atoms neighboring the collision site can acquire sufficient energy for mobility enhancement. When this enhancement is sufficient to overcome surface diffusion barrier, the atoms are able to reach sites, which are conducive to the stable crystalline growth. As the N_2 partial pressure increases, the mobility of Mo particles decreases. This can be understood by the fact that nitrogen can act as a roadblock to the diffusing Mo or can trap diffusing Mo, or can serve as a nucleation site for lattice defects. Therefore, the growing Mo particles may not be sufficiently mobile to migrate to the preferred sites for perfect crystallization growth. As shown in Fig. 5 (see spectra B and C), the (111) and (200) diffraction peaks observed in XRD $\theta-2\theta$ measurements are broader and their intensities are relatively weak, indicating that the degree of ordering for the as-deposited films is lower, probably due to small crystallite size and distortion of the lattice structure.

The lattice parameter for the as-deposited Mo_2N film is higher than the corresponding bulk value of 0.4163 nm (Fig. 5). A continuous shift of the lattice parameter towards higher values of x is also evidenced (not shown). The crystal structure of Mo_2N is B1–NaCl type where the Mo atoms occupy the positions of the fcc lattice points and N atoms occupy 50% of the total octahedral sites. In the case of overstoichiometric films, the excessive nitrogen could possibly be occupying these vacant octahedral sites, resulting in an expansion of the lattice. However, the possibility of the presence of excess nitrogen at the interstitial sites and grain boundaries also cannot be completely ruled out.

The annealing used in the present investigation presumably serves only to activate atom diffusion, structure conversion, and phase ordering [23,24]. After high temperature annealing, adatom mobilities in the film are sufficiently high to form a well-ordered single-phase structure of Mo_2N. We wish to point out that no significant loss of nitrogen was found for films near or below stoichiometry of Mo_2N after annealing up to 750 °C (Fig. 6).

4.3. Chemical bonding and film density

The chemical bonding configuration of the films was characterized by XPS. The results reveal that the binding energies of the Mo $3d_{5/2}$ and Mo $3d_{3/2}$ electrons in the crsytallized MoN_x films deposited at 4 mTorr (12 mTorr) were 228.1 (228.3) and 231.4 (231.5) eV, respectively (Fig. 7a). This indicates that the Mo 3d peaks relative to those (centered at 227.8 and 231.0 eV) in bcc Mo were shifted to higher binding energies. No significant difference in binding energies between the analyzed samples was found. This suggests that the chemical bonding configuration of the Mo films before and after nitridation is different. The observed N 1s binding energies at 397.2 eV for 4 mTorr case and 397.5 eV for 12 mTorr case (Fig. 7b) are close to the values reported for TiN (396.9 eV), W_2N (397.3 eV), Zr_3N_4 (397.2 eV), Ta_3N_5 (396.9 eV) and other early transition metal nitrides [25,26]. In addition, since the N 1s peak is enveloped in that of Mo 3p, the peaks measured at 394.5 eV for 4 mTorr case and 394.6 eV for 12 mTorr case are actually due to Mo $3p_{3/2}$ electrons.

At lower growth temperatures, the films may have amorphous or disordered crystalline phases and their crystalline quality is inferior due to poor surface mobility of the adatoms. In addition, amorphous or poor ordered crystalline phases usually have lower densities than their ordered crystalline counterparts. This has been evidenced by measuring the density of two MoN_x samples via the free electron model and the bulk plasmon energies determined by EELS (Fig. 8b). The film density reached a plateau after annealing at about 500 °C, and then remained almost constant. Film densification is due to crystallization induced at higher temperature annealing, in good agreement with our XRD results described above. Our measurement of 9.45×10^3 and 9.2710^3 kg m^{-3} for the MoN_x films containing 35 at.% N prepared at 4 and 12 mTorr, respectively, after annealing to 600 °C is consistent with the mass density value of Mo_2N (9.5×10^3 kg m^{-3}).

5. Conclusions

Mechanical stresses and microstructure of MoN_x thin films, with $0 \leq x \leq 0.35$, prepared by reactive magnetron sputtering under different total sputtering-gas pressures have been studied in situ using a wafer curvature-based technique and ex situ using TEM, TED, XRD, XPS and EELS. Four conclusions are strongly supported by the results.

(1) The Mo film stresses strongly depended on the Ar sputtering pressure and changed from highly compressive to highly tensile in a relatively narrow pressure range of 6–12 mTorr. For pressures exceeding $\sim$40 mTorr, the stress in the film was nearly zero. Cross-sectional TEM evidence indicated that the compressively stressed films contained a dense microstructure without any columns, while the films having tensile stress had a very columnar microstructure. High sputtering-gas pressure conditions yielded dendritic-like film growth, resulting in complete relaxation of the mechanical tensile stresses.

(2) The properties of the deposited MoN_x films, with $0 \leq x \leq 0.35$, depended not only on the nitrogen partial pressure in $Ar-N_2$ gas mixtures but also on the total sputtering-gas pressure. Mechanical stresses and microstructure of the films were clearly correlated.

(3) The formation of either a two-phase structure consisting of Mo_2N and bcc Mo or a single-phase structure of Mo_2N after annealing was related to the initial nitrogen concentration in the films. Once the Mo_2N phase was formed, the density, microstructure and bonding feature were similar and insensitive to the total sputtering pressure used in this study.

(4) An average column width of $\sim$15–20 nm was observed for films near stoichiometry of Mo_2N.

(5) TED with a PDF analysis is a useful tool in the unambiguous identification of Mo–N and Mo–Mo bonding in the films.

Acknowledgements

Part of this work was supported by a Grant of the City University of Hong Kong under project Number 9001184. The author is very grateful to Professor Y.-W. Mai for many stimulating discussions on residual stress analysis. Access to and use of some facilities in the Australian Key Center for Microscopy and Microanalysis, The University of Sydney, is much appreciated.

References

[1] L.E. Toth, Transition Metal Carbides and Nitrides, Academic, New York, 1971.
[2] T. Nakajima, T. Shirasaki, J. Electrochem. Soc. 144 (1997) 2096.
[3] F. Klabunde, M. Löhmann, J. Bläsing, T. Drüsedau, J. Appl. Phys. 80 (1996) 6266.
[4] J.D. Wu, C.Z. Wu, Z.M. Song, F.M. Li, Thin Solid Films 311 (1997) 62.
[5] J.C. Chuang, S.L. Tu, M.C. Chen, Thin Solid Films 346 (1999) 299.
[6] L.P. Kendig, Z.U. Rek, S.M. Yalisove, J.C. Bilello, Surf. Coatings Technol. 132 (2000) 124.
[7] D. Windt, J. Vac. Sci. Technol. A 18 (2000) 980.
[8] S.L. Roberson, D. Finello, R.F. Davis, Surf. Coatings Technol. 102 (1998) 256.
[9] S.L. Roberson, D. Finello, R.F. Davis, Thin Solid Films 324 (1998) 30.
[10] J.Y. Lee, S.R. Jeon, J.W. Park, J. Mater. Sci. Lett. 15 (1996) 1495.
[11] H. Kattelus, J. Koskenala, A. Nurmela, A. Niskanen, Microelec. Eng. 60 (2002) 97.
[12] V.P. Anitha, S. Major, D. Chandrashekharam, M. Bhatnagar, Surf. Coatings Technol. 79 (1996) 50.
[13] Y.G. Shen, Y.W. Mai, Q.C. Zhang, D.R. McKenzie, W.D. FcFall, W.E. McBride, J. Appl. Phys. 87 (2000) 177; 88 (2000) 1380.
[14] Y.G. Shen, Y.W. Mai, W.E. McBride, D.R. McKenzie, Q.C. Zhang, Appl. Phys. Lett. 75 (1999) 2211.
[15] J.A. Thornton, D.W. Hoffman, Thin Solid Films 171 (1989) 5.
[16] P. Gouy-Pailler, Y. Pauleau, J. Vac. Sci. Technol. A 11 (1993) 96.
[17] M.A.E.I. Khakani, M. Chaker, B.L.e Drogoff, J. Vac. Sci. Technol. A 16 (1998) 885.
[18] M. Hansen, Constitution of Binary Alloys, second ed, McGraw-Hill, New York, 1958.
[19] A.J.C. Wilson (Ed.), International Tables for Crystallography, vol. C, Kluwer Academic Publisher, The Netherlands, 1995.
[20] R. Fix, R.G. Gordon, D.M. Hoffman, Thin Solid Films 288 (1996) 116.
[21] R.F. Egerton, Electron Energy Loss Spectroscopy in the Electron Microscope, second ed, Plenum, New York, 1996.
[22] J.A. Thornton, D.W. Hoffman, Thin Solid Films 171 (1989) 5.
[23] Y.G. Shen, J. Yao, D.J. O'Connor, B.V. King, R.J. MacDonald, Phys. Rev. B 56 (1997) 9894.
[24] Y.G. Shen, A. Qayyum, D.J. O'Connor, B.V. King, Phys. Rev. B 58 (1998) 10025.
[25] R. Fix, R.G. Gordon, D.M. Hoffman, Chem. Mater. 3 (1991) 1138.
[26] R. Fix, R.G. Gordon, D.M. Hoffman, Chem. Mater. 5 (1993) 614.